Published online 19 June 2015

Nucleic Acids Research, 2015, Vol. 43, No. 19 ***e127***
doi: 10.1093/nar/gkv624

Simultaneous live imaging of the transcription and nuclear position of specific genes

Hiroshi Ochiai[1,*], Takeshi Sugawara[1] and Takashi Yamamoto[1,2]

[1]Research Center for the Mathematics on Chromatin Live Dynamics (RcMcD), Hiroshima University, Higashi-Hiroshima 739-8530, Japan and [2]Department of Mathematical and Life Sciences, Graduate School of Science, Hiroshima University, Higashi-Hiroshima 739-8526, Japan

Received February 26, 2015; Revised June 02, 2015; Accepted June 04, 2015

ABSTRACT

The relationship between genome organization and gene expression has recently been established. However, the relationships between spatial organization, dynamics, and transcriptional regulation of the genome remain unknown. In this study, we developed a live-imaging method for simultaneous measurements of the transcriptional activity and nuclear position of endogenous genes, which we termed the 'Real-time Observation of Localization and EXpression (ROLEX)' system. We demonstrated that ROLEX is highly specific and does not affect the expression level of the target gene. ROLEX enabled detection of sub-genome-wide mobility changes that depended on the state of *Nanog* transactivation in embryonic stem cells. We believe that the ROLEX system will become a powerful tool for exploring the relationship between transcription and nuclear dynamics in living cells.

INTRODUCTION

Recent progress in chromosome conformation capture (3C)-related technologies (4C, 5C and Hi-C) revealed the three-dimensional genomic organization of several cell types from diverse organisms, including mouse embryonic stem cells (mESCs), and many long-range genomic interactions involved in the regulation of gene expression (1–4). Although 3C-related techniques can generally be used to obtain the average probability of genomic interactions in a large number of cells, the distances between specific genomic regions are variable among individual cells (5). Such variation in the nuclear organization between cells might contribute to cell-to-cell variability in gene expression (6). Although several attempts have been made to understand the relationships between gene expression and highly dynamic nuclear organization in cell populations (7,8), thus far, it has been difficult to gain insight into the relationship between gene expression and its dynamic behavior in the cell nucleus.

Here, we describe the establishment of the Real-time Observation of Localization and EXpression (ROLEX) system for live imaging of the transcriptional state and nuclear position of a specific endogenous gene. In this system, the insertion of a 1.3-kb long MS2 repeat into a specific gene of interest not only enables the visualization of gene transcription using the MS2 coat protein fused to the tandem near-infrared red-fluorescent protein (tdiRFP) (MCP-tdiRFP) (9), but also allows for the determination of the gene position in the nucleus using a Cas9 mutant with undetectable endonuclease activity (dCas9) fused to the green fluorescent protein (GFP) (dCas9-GFP) and three single-guide RNAs (sgRNAs) (10). Using this system, we detected sub-genome-wide mobility changes that depended on the state of *Nanog* transactivation in mESCs. This system will help to overcome the current knowledge gap regarding the association between gene transcription and nuclear dynamics by increasing our insight into the fundamental mechanisms of genomic organization and gene regulation.

MATERIALS AND METHODS

Plasmid construction

Plasmids were constructed in the following manner: pPB-LR5-CAG-MCP-tdiRFP670-IRES-Neo, was constructed by digesting pBSKΔB-CAG-MCP-tdiRFP670-IRES-Neo (Addgene [http://www.addgene.org] plasmid 62345) with BsmBI and inserting the CAG-MCP-tdiRFP670-IRES-Neo cassette into the NheI/SalI site of the pPB-LR5 (11); pPB-LR5-TRE-dCas9-mNeonGreen (12) (Allele Biotechnology, San Diego, CA, USA) was built by digesting pBSKΔB-TRE-dCas9-mNeonGreen with BbsI and inserting the TRE-dCas9-mNeonGreen cassette into the NheI/SalI site of pPB-LR5; and pPB-LR5-CAG-rtTA2sM2-IRES-tTSkid-IRES-Neo was constructed by digesting pBSKΔB-CAG-rtTA2sM2-IRES-tTSkid-IRES-Neo (Addgene plasmid 62346) with BsmBI and inserting the CAG-rtTA2sM2-IRES-tTSkid-IRES-Neo cassette into the NheI/SalI site of pPB-LR5. The pCAG-hyPBase

*To whom correspondence should be addressed. Tel: +81 82 424 5529; Fax: +81 82 424 5529; Email: ochiai@hiroshima-u.ac.jp

© The Author(s) 2015. Published by Oxford University Press on behalf of Nucleic Acids Research.
This is an Open Access article distributed under the terms of the Creative Commons Attribution License (http://creativecommons.org/licenses/by-nc/4.0/), which permits non-commercial re-use, distribution, and reproduction in any medium, provided the original work is properly cited. For commercial re-use, please contact journals.permissions@oup.com

plasmid was constructed by replacing the CMV promoter of the pCMV-hyPBase plasmid (13) with a CAG promoter.

To construct the pKLV-U6gRNA-EF(BbsI)-PGKpuro2ABFP plasmid (Addgene plasmid 62348), which is a vector for optimized sgRNA expression (10), the human U6 promoter-BbsI-BbsI-optimized sgRNA cassette was inserted into the ApaI/BamHI site of the pKLV-U6gRNA(BbsI)-PGKpuro2ABFP plasmid (14) (plasmid 50946, Addgene; deposited by Kosuke Yusa). Individual sgRNA expression vectors were constructed as described previously (15). The list of sequences of the oligonucleotides used is given in Supplementary Table S1.

To construct the pKLV-PGKpuro2ABFP plasmid, which is an sgRNA empty vector, we performed inverse PCR using primers pKLV-F and pKLV-R (Supplementary Table S2) and pKLV-U6gRNA-EF(BbsI)-PGKpuro2ABFP as a template, followed by the digestion of the PCR product by EcoRI and subsequent self-ligation.

To construct pPB-LR5-CAG-mRuby2-H2A-IRES-Neo, pPB-LR5-CAG-CENP-A-mRuby2-IRES-Neo, and pPB-LR5-CAG-TRF1-mRuby2-IRES-Neo, the MCP-tdiRFP670 cDNA of pPB-LR5-CAG-MCP-tdiRFP670-IRES-Neo was replaced with mRuby2-H2A, CENP-A-mRuby2, or TRF1-mRuby2 cDNA molecules, respectively.

The clustered regularly interspaced short palindromic repeat (CRISPR)/Cas9 nickase (Cas9n), and sgRNA expression vectors px335-Oct4L and px335-Oct4R were constructed using the pX335-U6-Chimeric_BB-CBh-hSpCas9n(D10A) vector (plasmid 42335, Addgene; deposited by Feng Zhang) (16) as previously described (15). The list of sequences of the oligonucleotides that we used is given in Supplementary Table S1.

Targeting vectors containing 2A-loxP-hsvTK-2A-Hyg-loxP-24×MS2 (pTV-Oct4-TK-HMS, Addgene plasmid 62351) were constructed by PCR and standard cloning techniques as described previously (17). In order to avoid cutting the 5′-homology arm, we introduced multiple synonymous nucleotide substitutions into the CRISPR/Cas9n target sites (see Supplementary Figure S1).

Cell culture

Mouse embryonic stem cells (mESCs) were cultured as described previously (17). Briefly, mESC lines [NMP (17), NMP-R, Bruce 4 C57BL/6 mESCs, OM and OM-R cells] were cultured in 2i conditions (Dulbecco's modified Eagle's medium [DMEM]; 15% fetal bovine serum [FBS]; 0.1 mM β-mercaptoethanol, 1× MEM nonessential amino acids, 2 mM L-alanyl-L-glutamine solution, 1000 U/ml leukemia inhibitory factor [LIF], 20 μg/ml gentamicin, 3 μM CHIR99021 and 1 μM PD0325901) on a 0.1% gelatin-coated dish. Prior to each experiment, cells were passaged twice and cultured in 2i conditions as well as in standard conditions (DMEM, 15% FBS, 0.1 mM β-mercaptoethanol, 1 × MEM nonessential amino acids, 2 mM L-alanyl-L-glutamine solution, 1000 U/ml LIF, and 20 μg/ml gentamicin).

Gene targeting

The day before transfection, C57BL/6 mESCs (5×10^4) were plated onto 24-well plates, in order to generate the $Oct4^{MS2/WT}$ cell line. The cells were then transfected on the next day with 1 μg pTV-Oct4-TK-HMS, 250 ng Cas9n and sgRNA expression vectors (px335-Oct4L and px335-Oct4R) using Lipofectamine 2000 (Life Technologies, Gaithersburg, MD, USA), according to the manufacturer's instructions. After another 24 h, cells were transferred to 10-cm plates, incubated for 72 h, and then subjected to Hygromycin selection (150 μg/ml). Homologous recombination was verified by using PCR and Southern blotting. The synonymous nucleotide substitutions, which were the same as those in the targeting vector, were introduced in a non-transgene-integrated allele of the obtained clone ($Oct4^{TH\text{-}MS2/WT}$) (Supplementary Figure S1). Then, in order to excise the selection cassette flanked by *loxP* sites, 500 ng Cre expression vector (pCAG-Cre [plasmid 13775, Addgene; deposited by Connie Cepko]) (18) was transfected into the obtained clone ($Oct4^{TH\text{-}MS2/WT}$). The genotype of the resultant ganciclovir-resistant mESC ($Oct4^{MS2/WT}$, OM clone) was confirmed by Southern blotting, as described previously (19). Our data showed that cell lines expressed undifferentiated embryonic stem-cell markers SSEA-1, Nanog, and Oct4, as shown in Supplementary Figure S1. Immunofluorescence was performed as described by Ochiai *et al.* (17).

For the ROLEX system, NMP and OM cells (1×10^4) were plated onto a μ-Slide 8-well (Ibidi, Martinsried, Germany) 1 day before transfection. On the next day, the cells were transfected with 200 ng pPB-LR5-CAG-MCP-tdiRFP670-IRES-Neo, 50 ng pPB-LR5-TRE-dCas-mNeonGreen, 50 ng pPB-LR5-CAG-rtTA2sM2-IRES-tTSkid-IRES-Neo, and 50 ng pCAG-hyPBase using Lipofectamine 2000. After 96 h, the cells were transferred onto a μ-Dish 35 mm Grid-500 (Ibidi), incubated for 72 h, and then subjected to G418 selection. After a week-long incubation period, cells were treated with doxycycline (Dox [100 ng/ml]) for 12 h and used for live imaging. Colonies with mNeonGreen and tdiRFP670 signals were identified and used for further analysis.

Sequential RNA and DNA-FISH

Trypsinized cells were transferred onto Laminin-511 (BioLamina, Stockholm, Sweden)-coated glass slides and cultured overnight at 37°C and 5% CO_2. Cells were washed with phosphate-buffered saline (PBS), fixed with 4% paraformaldehyde in PBS for 10 min, followed by washing twice with PBS and subsequent treatment with PBS-containing Hoechst 33342 nucleic acid stain (1:1000) (Life Technologies, Gaithersburg, MD, USA) for 10 min. Images were acquired using the following instruments: an Olympus IX83 microscope (Olympus, Tokyo, Japan) with a CSU-W1 confocal unit (Yokogawa, Tokyo, Japan); a 100× Olympus oil immersion objective of 1.40 NA; an iXon3 EMCCD camera with 512 × 512 pixels (Andor, Belfast, UK) with laser illumination at 405 nm for Hoechst 33342, 488 nm for dCas9-GFP, and 637 nm for MCP-tdiRFP. In this setting, the pixel size was 160 nm. Images were analyzed using Metamorph software (Universal Imaging Corporation,

West Chester, PA); 76 z-planes per site spanning 15 μm (z-step = 200 nm) were acquired. Subsequently, cells were subjected to 3D-RNA-FISH as previously described, but with some modifications (20). Briefly, cells were washed twice with PBS and then permeabilized in 0.1% saponin/0.1% Triton X-100/2 mM ribonucleoside vanadyl complex in PBS for 10 min at room temperature (RT). Following two washes with PBS, cells were incubated for 20 min in 20% glycerol/PBS at RT and stored in 50% glycerol/PBS at −20°C for at least 1 day. After the incubation, cells were recalibrated at RT in 20% glycerol/PBS, and subjected to three successive freeze/thaw cycles in liquid nitrogen (20). Thereafter, cells were washed twice with PBS for 5 min each at RT, incubated in 0.1 M HCl for 30 min at RT, washed once again with PBS for 5 min at RT, permeabilized in 0.5% saponin/0.5% Triton X-100 in PBS for 30 min at RT, washed two more times with PBS for 5 min per wash at RT, and then equilibrated in 50% formamide/2× SSC for 10 min at RT. Next, the cells were hybridized to a pre-denatured MS2 probe set (17) using the hybridization buffer containing 1× saline sodium citrate (SSC), 10% dextran sulfate, and 50% formamide. Hybridization was performed for 16 h at 37°C in a moist chamber. Subsequently, the cells were washed in 2× SSC for 5 min at RT, 50% formamide/2× SSC for 15 min at 45°C, 2× SSC for 5 min at 45°C, and then 2× SSC for 5 min at RT, followed by a wash in 2× SSC with Hoechst 33342 (1:1000) for 10 min at RT. Hybridized cells were mounted in catalase/glucose oxidase-containing mounting media, as described previously (17). Images were taken as outlined above using laser illumination set at 405 nm for Hoechst 33342 and at 561 nm for MS2 probes. Then, the cells were subjected to 3D-DNA-FISH, as described previously (20). The BAC clones RP23-19O18 and RP24-367I6 (CHORI BACPAC Resources) were used as DNA-FISH probes for *Nanog* and XA1.1, respectively.

Image segmentation, nuclear identification, and quantification of fluorescence intensity were conducted using the automated open-source program CellProfiler (http://www.cellprofiler.org) (21). The parameters used for nuclear identification are listed in Supplementary Table S3.

Single-molecule FISH (smFISH)

Trypsinized cells were transferred onto laminin-511-coated glass slides and cultured for 3 h at 37°C and 5% CO_2. Cells were washed with PBS, fixed with 4% paraformaldehyde in PBS for 10 min, washed two more times with PBS, and then treated with PBS containing Hoechst 33342 (1:1000) for 10 min. Images were obtained using an Olympus IX83 microscope with a CSU-W1 confocal unit; a 60× Olympus oil immersion objective of 1.42 NA; and an iXon3 EMCCD camera with 512× 512 pixels, with laser illumination at 405 nm for Hoechst 33342, 488 nm for dCas9-GFP, and 637 nm for MCP-tdiRFP. In this setting, pixel size was 266 nm. We acquired 76 z-planes per site spanning 15 μm (z-step = 200 nm). Subsequently, cells were washed twice with PBS and permeabilized in 70% ethanol at 4°C overnight. Following a wash with 10% formamide dissolved in 2× SSC, the cells were hybridized to an MS2 probe set (17) for 4 h at 37°C in a moist chamber using a hybridization buffer containing 2 × SSC, 10% dextran sulfate, and 10% formamide. After hybridization, the cells were first washed in a solution containing 10% formamide in 2× SSC, followed by a second wash in 10% formamide in a 2× SSC with Hoechst 33342 (1:1000). Hybridized cells were mounted in a mounting media containing catalase/glucose oxidase, as previously described (17). Images were acquired as outlined above using laser illumination set at 405 nm for Hoechst 33342 and 561 nm for MS2 probes. Image analysis was performed using previously described methods (17).

Western blot analysis

The NMP-R mESCs (1×10^5) were plated onto 12-well plates. On the following day, the cells were transfected with either 2 μg of sgRNA expression vectors or 1400 and 600 ng of MS2 and XA1.1 sgRNA expression vectors, respectively, using Lipofectamine 2000. After a 12-h period, the cells were treated with puromycin (2 μg/ml) and Dox (25 ng/ml). After incubation for another 24 h, the cells were cultured in the Dox-containing medium overnight at 37°C and 5% CO_2 and then lysed in the lysis buffer (0.5% Triton X-100, 150 mM NaCl, 20 mM Tris–HCl, pH 7.5) on the following day. Then, the lysates were incubated on ice for 40 min, and clarified by centrifugation. The extracted proteins were analyzed by 10% (wt/vol) SDS-PAGE and transferred onto Immobilon transfer membranes (Millipore, Billerica, MA, USA) for immunoblotting analyses. The primary antibodies used were the rat anti-mouse Nanog monoclonal antibody (mAb) (eBioscience, San Diego, CA, USA) and rabbit anti-GAPDH mAb (Cell Signaling Technology, Danvers, MA, USA).

Reverse transcription quantitative PCR

The NMP-R mESCs were transfected with sgRNA expression vectors and treated as described above. Cells were then transferred onto 96-well plates, 6 h before RNA extraction. Total RNA was isolated from cells using a SuperPrep Cell Lysis Kit (Toyobo, Osaka, Japan) for quantitative PCR (qPCR) and for reverse transcription (RT)-PCR according to the manufacturer's protocol. Total RNA was converted to cDNA using a SuperPrep RT Kit for qPCR (Toyobo). qPCR was performed with the Stratagene Mx3000p (Agilent Technologies, Palo Alto, CA, USA) using the THUNDERBIRD SYBR qPCR Mix (Toyobo). The threshold cycle (Ct) value was normalized with the housekeeping gene *Gapdh* and the relative fold change was computed by the ΔΔCt method (22). Primer sequences are listed in Supplementary Table S2.

Live imaging

The NMP-R and OM-R mESCs (5×10^4) were plated onto 24-well plates on the day before transfection, for simultaneous live imaging of transcription and intranuclear positioning of specific genes using the ROLEX system. Cells were then transfected with 1 μg of sgRNA expression vectors on the following day using Lipofectamine 2000. Cells were transfected with a mixture of 700 and 300 ng of MS2 and XA1.1 sgRNA expression vectors, respectively, for the simultaneous imaging of MS2 and XA1.1 loci. After 12 h,

the cells were treated with puromycin (2 μg/ml) and Dox (100 or 25 ng/ml) for another 24 h. The cells were subsequently trypsinized and transferred onto a μ-Slide 8-well coated with Laminin-511 and cultured overnight at 37°C and 5% CO_2 in the Dox-containing medium. Then, after changing the Dox medium, live images of the cells were acquired using an Olympus IX83 microscope with a CSU-W1 confocal unit and a 100× Olympus oil-immersion objective of 1.40 NA. Fluorescence images were captured using an iXon3 EMCCD camera with 512 × 512 pixels, equipped with a 488 and 637 nm laser, a stage-top microscope incubator (5% CO_2; 37°C; Tokai Hit, Shizuoka, Japan), and an ASI MS-2000 piezo stage (ASI, Lyon, France). In this setting, the pixel size was 160 nm. Images were analyzed using Metamorph software; 46-z planes per site spanning 9 μm (z-step = 200 nm) were acquired with a 10 s interval time for 500 s. Acquired images were filtered with a one-pixel diameter 3D Gaussian Blur filter using ImageJ software (National Institutes of Health, Bethesda, MD). The dCas9-GFP images obtained were subjected to background subtraction using an ImageJ plugin with a rolling ball radius of five pixels. Fluorescent spots were detected using the Imaris software (Bitmap, Zurich, Switzerland) 'Spot' function with a spot diameter set at 0.8 μm (i.e., semi-automatic detection). The nucleus center of mass was estimated from nuclear localized MCP-tdiRFP fluorescence using ImarisCell (Bitmap), with the Cell Smooth Filter Width and Cell Background Subtraction Width parameters set at 1 and 0.64 μm, respectively.

Mean squared displacement analysis

The mean squared displacement (MSD) was calculated as the average change in distance between the *MS2* and XA1.1 loci, or between the nuclear center of mass and each genomic locus over all possible combinations of time points separated by the lag time Δt; $[d(t) - d(t + \Delta t)]^2 = 4D\Delta t$, where D is the diffusion coefficient (23). The diffusion coefficient D of a particle is proportional to the initial slope m on an MSD curve (24). However, in general, the free movement of an object can be confined in a nuclear or cellular compartment (25). This implies that the distance of any two points of the trajectory cannot exceed the maximal extension of the confining volume. Therefore, the MSD curves must reach a plateau at large time windows. Nonetheless, one can still use the initial slope m of MSD curve to compare the intrinsic mobility of different objects or one object under different conditions. Initial slopes m were obtained by a least-square linear fitting of the first half of points (10 – 250 s). Diffusion constant D were then determined $D = m/4$. To compare the diffusion coefficients under various conditions, we used a one-tailed Student's t-test.

RESULTS

Specificity of the ROLEX system

To establish the imaging method for simultaneous measurement of the transcriptional activity and nuclear position of an endogenous gene, which we termed the ROLEX system (Figure 1A), we first chose the mESC line (NMP) in which MS2 and PP7 repeats are integrated into each *Nanog* allele (Figure 1B) (17). Transcribed MS2 and PP7 sequences derived from MS2 and PP7 bacteriophages, correspondingly, form stem-loop structures which are known to be bound respectively by the MS2 coat protein (MCP) and PP7 coat protein (PCP) as dimers (9). Therefore, the integration of the 24 tandem MS2 and PP7 sites into a specific gene of interest and the expression of MCP and PCP fused to fluorescent proteins (MCP-FP and PCP-FP), enables a visualization of mRNA transcription as bright spots in the nucleus (9). We previously demonstrated that the MS2/MCP-FP system can be used to quantitate transcriptional dynamics in mESCs, although a tendency toward the nucleolar localization of PCP-FP prevents precise quantification of its transcription dynamics, at least in mESCs (17). Integration of MS2 and PP7 repeats into each *Nanog* allele in NMP mESCs enables monitoring of allele-specific transcription and verification of the ROLEX system's specificity by allele-specific RNA-FISH (17). We created a clonal mESC line (NMP-R) that constitutively expressed MCP-tandem near-infrared (tdiRFP) and stably expressed dCas9-GFP from a tetracycline (tet) inducible system using the *piggyBac* transposon that enables highly efficient transgenesis (Figure 1C) (11,13). As expected, treatment with the system's inducer Dox at a concentration of 100 ng/ml increased the number of cells with GFP fluorescence intensity above the background over time (Supplementary Figure S2). However, expression levels of dCas9-GFP varied considerably among cells (Supplementary Figure S2). We recloned several cell lines from NMP-R to avoid the possibility of genetic heterogeneity, but a significant variability in expression levels was still observed (data not shown).

To investigate whether dCas9-GFP localizes to specific sub-nuclear domains in NMP-R cells in an sgRNA-dependent manner, we introduced telomere or minor satellite (MiSat) sgRNA expression vectors with nuclear (histone H2A-RFP) or subnuclear markers (centromere marker CENP-A-RFP; telomere marker TRF1-RFP) into NMP-R cells. We applied an optimized sgRNA design ($sgRNA^{(F+E)}$) that improves imaging efficiency (10). In 12 h post-transfection, we treated cells with puromycin and Dox (25 ng/ml) for 24 h. Because sgRNA expression vectors contain the puromycin resistance gene, transient treatment with puromycin eliminates untransfected cells. After another 12-h treatment with Dox, we examined the localization of dCas9-GFP (Figure 1D–F). Consistent with a previous report, dCas9-GFP without sgRNA tended to localize in the nucleoli (10). In cells transfected with MiSat sgRNA and centromere marker CENP-A-RFP expression vectors, dCas9-GFP and CENP-A-RFP signals were well co-localized (Figure 1E), which is consistent with mouse minor satellite DNA genetically mapping to the centromere (26). Moreover, in cells transfected with telomere sgRNA and telomere marker TRF1-RFP expression vectors, dCas9-GFP and TRF1-RFP signals were also mostly co-localized (Figure 1F). To further test the utility of CRISPR imaging, we designed 12 sgRNAs that theoretically targeted more than 300 sites within a tandem repeat region in the mouse chromosome locus XA1.1 and introduced these sgRNA expression vectors into NMP-R cells derived from male mice with only one X chromosome. Immediately after fixation, one bright spot in each individual cell was detected (Sup-

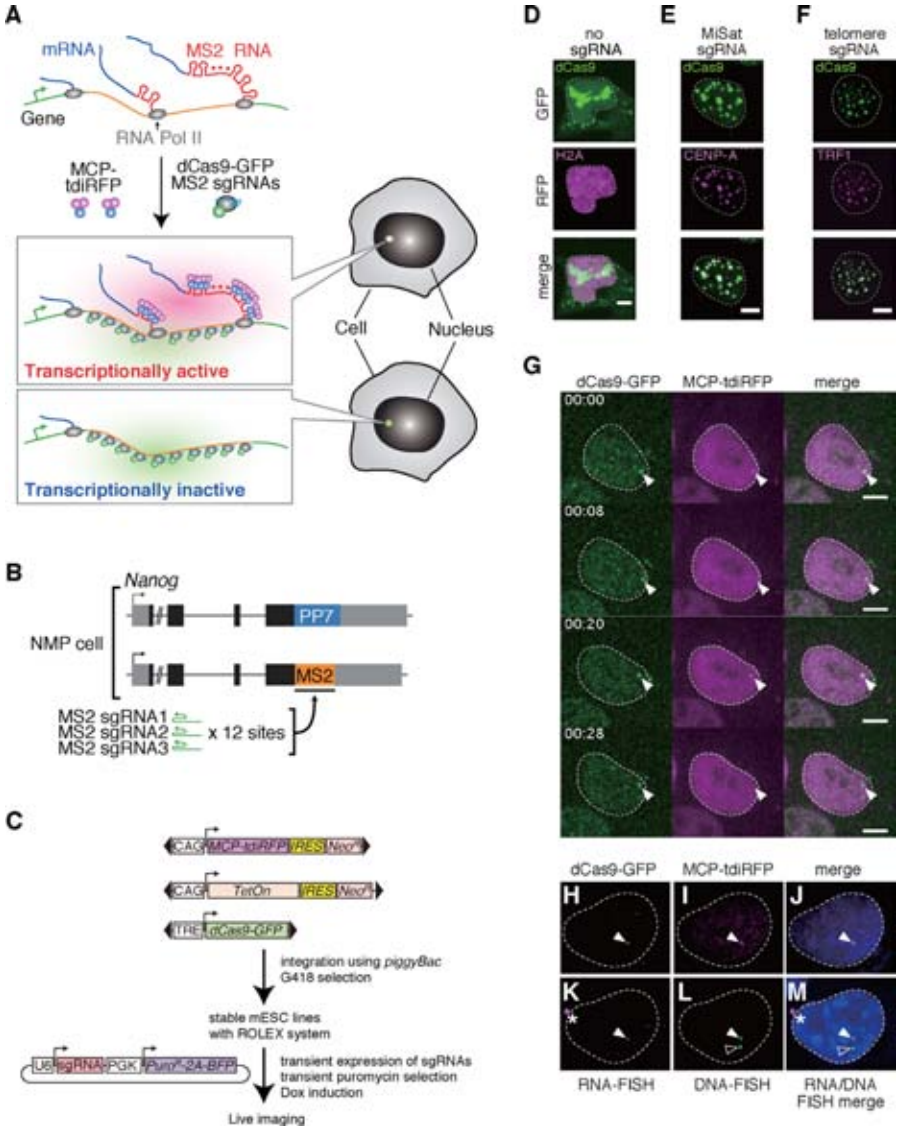

Figure 1. ROLEX system. (**A**) Schematic representation of the ROLEX system. Green, orange, blue and red lines represent the target DNA locus, integrated MS2 repeat, transcribed mRNA, and transcribed MS2 sequences, respectively. Nuclease-dead Cas9 (dCas9) fused to the green fluorescent protein (dCas9-GFP) with MS2 single-guide RNAs (sgRNAs) bind to the MS2 repeat. The MS2 coat protein (MCP) fused to the tandem near-infrared red fluorescent protein (tdiRFP) (MCP-tdiRFP) binds to each transcribed MS2 stem loop as a dimer. (**B**) The structure of *Nanog* in NMP cells. Grey, black, blue and orange boxes represent untranslated regions, coding sequences, and PP7 and MS2 repeats, respectively. Three types of MS2 sgRNAs theoretically bind to 36 sites within an MS2 repeat. (**C**) A schematic representation of the generation of cell lines integrated with vectors for the ROLEX system. The MCP-tdiRFP-internal ribosome entry site (IRES)-neomycin resistance gene (Neo^R) expression cassette driven by the CMV early enhancer/chicken beta actin (CAG) promoter, the *dCas9-GFP* cassette driven by the tet-responsive element (TRE) promoter, and the *TetOn-IRES-Neo*^{R} cassette driven by the CAG promoter were introduced with the *piggyBac* transposase into mouse embryonic stem cells (mESCs) and selected with G418. After Dox treatment, colonies with sufficient MCP-tdiRFP and dCas9-GFP fluorescent signals were picked up for further analysis. Then, sgRNA expression vectors, which contain the sgRNA expression cassette driven by the human U6 promoter (U6) and the puromycin resistance gene ($Puro^R$)- self-cleaving 2A peptide (2A)-blue fluorescent protein (BFP) expression cassette driven by the mouse *Pgk1* promoter (PGK), were transiently transfected into the established cells. Following Dox and puromycin treatment, the cells were subjected to live imaging. (**D**–**F**) sgRNA-dependent localization of dCas9-GFP. (**D**) Cells were transfected with the RFP-H2A expression vector and subjected to live imaging. dCas9-GFP (green) tended to localize in the nucleolus when there was no sgRNA. RFP-H2A (magenta) localized in the nucleus. (**E**) Cells were transfected with the minor satellite (MiSat) sgRNA expression vector and CENP-A-RFP expression vector, and subjected to live imaging. Signals of CENP-A (magenta), which is a specific histone H3 variant associated with MiSat, were clearly co-localized with dCas9 signals (green). (**F**) Cells were transfected with the telomere sgRNA expression vector and TRF1-RFP expression vector and subjected to live imaging. Signals of TRF1 (magenta), the telomere-specific protein, were clearly colocalized with dCas9 signals (green). (**D**–**F**) White dashed lines represent edges of nuclei. Scale bars: 5 μm. (**G**) Time-lapse microscopy of NMP-R cells transfected with the MS2 sgRNA expression vector. The maximum projected image sequence shows simultaneous visualization of transcription and localization of *Nanog-MS2* loci (arrowheads). Images were taken at 2-min intervals for 2 h. White dashed lines and arrowheads represent edges of nuclei and dCas9-GFP spots, respectively. Scale bars: 5 μm. (**H**–**M**) Specificity of the ROLEX system for *Nanog-MS2* (solid arrowheads) and *Nanog-PP7* (open arrowheads) confirmed by RNA and DNA fluorescent *in situ* hybridization (FISH). Nuclei were counter-stained with Hoechst 33342 (blue). Dashed lines represent edges of nuclei. (**H**–**J**) Images were taken immediately after fixation. (**J**) A merged image of dCas9-GFP (green), MCP-tdiRFP (magenta), and Hoechst 33342 (blue) is shown. (**K**–**M**) RNA (K) and DNA FISH (L). RNA FISH was performed using an MS2-specific probe (magenta). DNA FISH was performed using a probe for the *Nanog* locus (green). (**M**) A merged image of RNA and DNA FISH and Hoechst 33342 (blue) is shown. Asterisks represent non-specific signals.

plementary Figure S3). We confirmed that this dCas9-GFP spot co-localized with the DNA-FISH signal of the XA1.1 probe (Supplementary Figure S3). These results suggest that dCas9-GFP localized into specific sub-genomic regions in the sgRNA-dependent manner in NMP-R cells.

To fluorescently label the *Nanog-MS2* locus, we introduced three types of MS2 sgRNAs into NMP-R cells cultured in the medium containing two inhibitors (2i) of MEK and GSK3β, which increase *Nanog* expression in mESCs (27). These sgRNAs would theoretically bind to 36 sites within an MS2 repeat (Figure 1B, Supplementary Figure S4). By using live imaging, a single dCas9-GFP spot with discontinuous MCP-tdiRFP spot signals was observed in cells moderately expressing dCas9-GFP (Figure 1G, Supplementary Figure S5, and Movie 1). The discontinuous MCP-tdiRFP observed here is consistent with previous findings (17). Additionally, the dCas9-GFP and MCP-tdiRFP signals were mostly co-localized (Supplementary Figure S5). To confirm whether these signals corresponded to the *Nanog-MS2* gene locus, we performed sequential RNA- and DNA-FISH (Figure 1H–M). We observed that dCas9-GFP and MCP-tdiRFP spots were co-localized not only with the MS2 RNA-FISH signal but also with one of the two *Nanog*-locus DNA-FISH signals (Figure 1H–M). Furthermore, 6.11% ($n = 605$) of the cells analyzed were cells with a dCas9-GFP spot corresponding to one of the *Nanog* DNA-FISH signals (Supplementary Figure S6). Distribution of dCas9-GFP expression levels revealed that the MS2-targeted dCas9-GFP spot tended to be recognized in cells expressing dCas9-GFP at moderate levels (Supplementary Figure S6). These results suggest that the ROLEX system enables simultaneous imaging of the transcription and localization of a specific gene in the nucleus.

The dCas9-GFP/MS2-sgRNA complex has no apparent influence on target gene expression

In a previous study, dCas9 with an sgRNA recognizing the gene body was reported to occasionally reduce mRNA expression of the gene in an sgRNA-dependent manner (28). To check whether MS2 sgRNAs would affect *Nanog-MS2* mRNA expression levels, we introduced empty vectors as controls, and expression vectors for sgRNAs recognizing the telomere and tandem repeats on the X chromosome (XA1.1) (Supplementary Figure S3), and MS2 and/or PP7 sgRNAs into NMP-R cells with or without Dox treatment (25 ng/ml) and examined Nanog mRNA and protein levels. We found that introduction of MS2 or PP7 sgRNA expression vectors and the expression of dCas9-GFP did not affect *Nanog* mRNA or protein levels (Figure 2A and B). However, it is possible that the variability in dCas9-GFP expression levels among cells masks the effect on the *Nanog-MS2* mRNA expression (Supplementary Figure S2). Therefore, we performed smFISH using MS2 probes in NMP-R cells transfected with either empty vectors or MS2 sgRNA expression vectors, and quantified dCas9-GFP and *Nanog-MS2* mRNA expression levels. In this way, we confirmed that dCas9-GFP expression did not affect *Nanog-MS2* mRNA expression levels (Figure 2C and D). In addition, to investigate whether MS2 sgRNA/dCas9-GFP affects visualization of the MCP-tdiRFP transcriptional spot, we transfected MS2 or PP7 sgRNA expression vectors into NMP-R cells cultured in 2i conditions and counted approximately 100 cells with dCas9-GFP spots either with or without MCP-tdiRFP spots (Figure 2E–K). We found that approximately 20% of cells showed both dCas9-GFP and MCP-tdiRFP spots in cells transfected with either MS2 or PP7 sgRNA expression vectors (Figure 2E–K). This percentage is consistent with observations from a previous study (17), which suggests that the MS2 sgRNA/dCas9-GFP spot does not affect visualization of the MS2/MCP-tdiRFP transcriptional spot. These results demonstrate that the ROLEX system is a useful tool for the simultaneous visualization of transcription and nuclear position of a specific gene in living cells. We also observed that MS2 sgRNA/dCas9-GFP spot signals tended to decrease or disappear when a strong MCP-tdiRFP spot signal was detected (Supplementary Movies S2). This observation indicates that the MS2 sgRNA/dCas9-GFP complex might be unloaded without affecting *Nanog* expression because of RNA Pol II-mediated transcription. However, although a previous study suggested that sgRNA expression levels affect the efficiency of CRISPR imaging (10), sgRNA expression levels in individual cells are unknown in this study. Furthermore, in general, there is no obvious correlation between most of the MCP-tdiRFP and dCas9-GFP spot signal intensities (Supplementary Figure S5). Therefore, further analyses are required to understand the fate of the MS2 sgRNA/dCas9-GFP complex during transcription of the MS2 repeat sequence.

Relationships between transcriptional activity and nuclear dynamics of pluripotency-related genes

Next, we examined the relationships between transcriptional activity and nuclear dynamics of pluripotency-related genes *Nanog* and *Oct4* (also known as *Pou5f1*) using the ROLEX system. Compared to *Oct4*, *Nanog* is heterogeneously expressed in mESCs and it tends to be monoallelically transcribed (29,30). For the visualization of *Oct4*, we monoallelically introduced an MS2 repeat into the *Oct4* locus (Figure 3A, Supplementary Figure S1), and then established a cell line by introduction of vectors for the ROLEX system (OM-R cells). To analyze the dynamics of a specific nuclear locus, it is necessary to eliminate the confounding effects of nuclear movement and rotation. One way to accomplish this is to calculate the MSD, which is a robust method to analyze the general properties of an object's movement, by measuring the mean squared change in distance between the locus of interest and a reference locus, rather than measuring the change in the displacement of each locus (23,31). The initial slope of the MSD is proportional to the diffusion coefficient (D) of the loci (24). The more mobile two loci are, the faster the MSD value increases over time, and the steeper the MSD slope. In this study, we employed the XA1.1 locus as the reference because our male mESCs have only one X chromosome and can be easily labeled by XA1.1 sgRNAs (Supplementary Figure S3). Additionally, to analyze the dynamics of pluripotency-related genes, NMP-R and OM-R mESCs cultured in standard medium were transfected with MS2 and XA1.1 sgRNA expression vectors and subjected to live imaging at a rate of

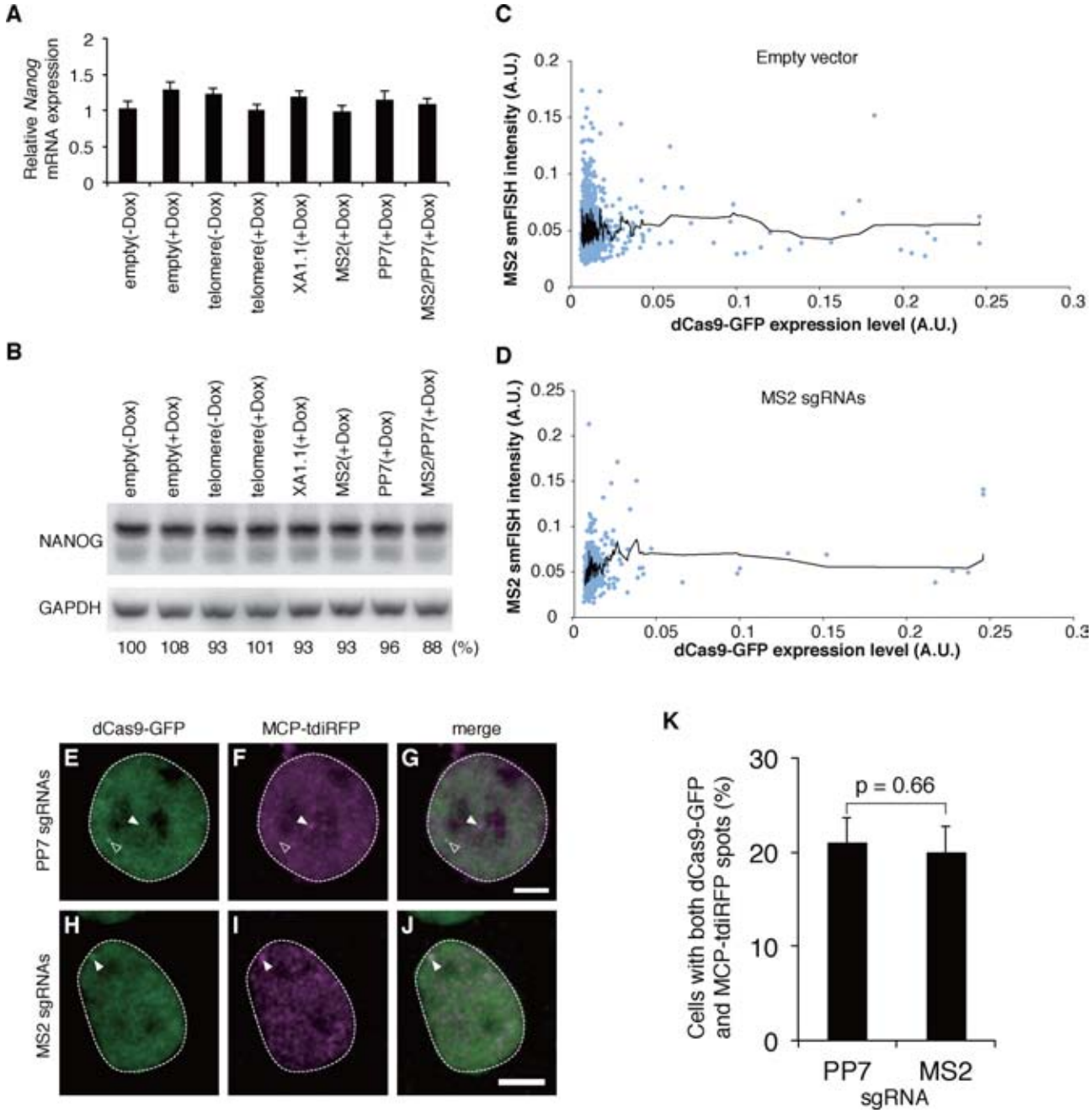

Figure 2. The absence of apparent influence of the dCas9-GFP/MS2-sgRNA complex on target gene expression. The ROLEX system did not affect target gene expression. (**A** and **B**) NMP-R cells were transfected with an empty vector, expression vectors for sgRNAs recognizing the telomere and tandem repeats on the X chromosome (XA1.1) as controls, and MS2 and/or PP7 sgRNAs, in presence (+Dox) or absence of Dox (-Dox). (**A**) Quantitative RT-PCR analysis of *Nanog* transcript levels between samples, normalized to the expression of *Gapdh* ($n = 3$). Error bars represent SD. (**B**) Western blot analysis of Nanog expression levels between samples; anti-GAPDH antibody was used as a loading control. The Nanog protein was reported to be detected as a ladder of bands in western blots because of alternative splicing and posttranslational modifications (51). Densitometric levels of Nanog bands normalized to those of GAPDH bands are shown beneath each lane. (**C** and **D**) Scatter plot of *Nanog-MS2* mRNA and dCas9-GFP expression levels. NMP-R cells were transfected with an empty vector (**C**) or MS2 sgRNA expression vectors (**D**), and subjected to single-molecule FISH (smFISH) using an MS2 probe set for quantification of dCas9-GFP and *Nanog-MS2* mRNA expression level at a single cell level. Black lines represent five-point moving averages. An increase or decrease of the *Nanog* mRNA expression level depending on the intensity of dCas9-GFP expression was not observed. (**E–K**) MS2 sgRNAs/dCas9-GFP spots do not affect visualization of MCP-tdiRFP spots. NMP-R cells were transfected with PP7 (**E–G**) or MS2 sgRNA expression vectors (**H-J**), and subjected to live imaging. (**E–J**) Representative images of cells harboring both dCas9-GFP (green) and MCP-tdiRFP (magenta) spots. Dashed lines, solid arrowheads, and open arrowheads represent edges of nuclei, *Nanog-MS2*, and *Nanog-PP7* loci, respectively. (**K**) Proportion of cells with both dCas9-GFP and MCP-tdiRFP spots ($n = 3$). Error bars represent SD. There was no significant difference between the two groups (two-tailed Student's *t* test).

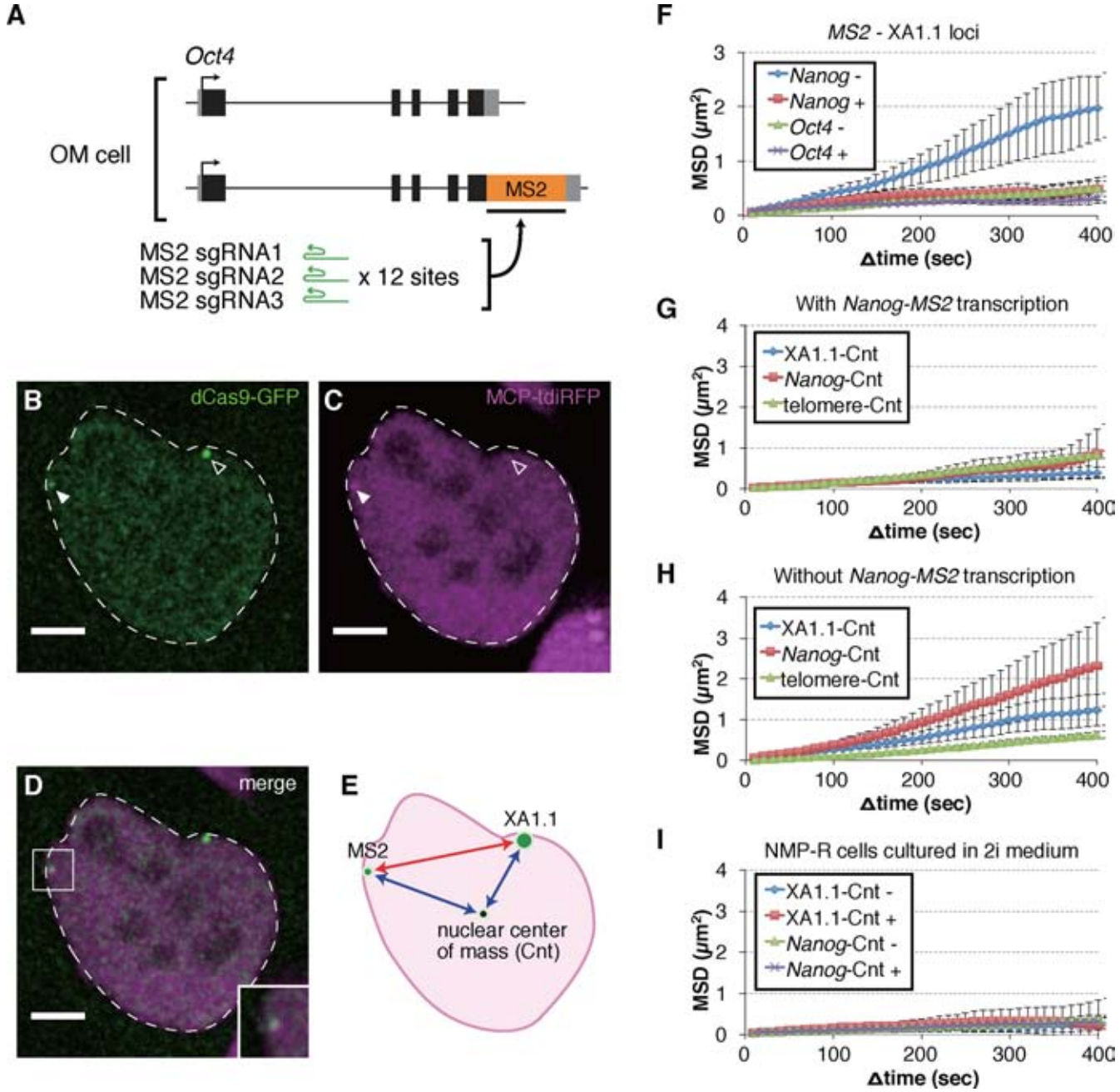

Figure 3. Mobility analysis of a specific genomic locus using the ROLEX system. (**A**) The structure of *Oct4* in an OM cell. Gray, black and orange boxes represent untranslated regions, coding sequences, and an MS2 repeat, respectively. Three types of MS2 sgRNAs theoretically bind to 36 sites within an MS2 repeat. (**B**–**D**) A representative image of an NMP-R cell transfected with MS2 and XA1.1 sgRNA expression vectors. The cell exhibited both dCas9-GFP (**B**) and MCP-tdiRFP (**C**) spots. The images show maximum intensity projections of stacks. The dashed line delineates the cell nucleus. The solid and open arrowheads are *Nanog-MS2* and XA1.1 loci, respectively. Scale bar: 5 μm. (**D**) A merged image of (**B**) and (**C**). Inset: boxed region at a higher magnification. (**E**) Schematic representation of a cell for the ROLEX system illustrating the mean square displacement (MSD) measurements. (**F**–**I**) Ensemble- and time-averaged MSD curves between (**F**) *MS2* and XA1.1 spots for NMP-R (*Nanog*) and OM-R (*Oct4*) cells with (+) or without (−) transcription during the 500-s imaging period (*Nanog*−, $n = 39$; *Nanog*+, $n = 13$; *Oct4*−, $n = 21$; and *Oct4*+, $n = 15$); (**G** and **H**) nuclear centre of mass (Cnt) and either *Nanog-MS2* (*Nanog*), XA1.1, or telomere spots for NMP-R cells with (**G**) (XA1.1-Cnt, $n = 39$; *Nanog*-Cnt, $n = 39$; and telomere-Cnt, $n = 266$ [about 10 spots each with higher fluorescence intensity of 25 cells]) or without (**H**) (XA1.1-Cnt, $n = 13$; *Nanog*-Cnt, $n = 13$; and telomere-Cnt, $n = 267$ [about 10 spots each with higher fluorescent intensity of 25 cells]) transcription during the imaging period; (**I**) Cnt and either *Nanog-MS2* (*Nanog*) or XA1.1 spots for NMP-R cells, cultured in 2i medium, with (+) or without (−) transcription during the imaging period (XA1.1-Cnt -, $n = 15$; *Nanog*-Cnt -, $n = 15$; XA1.1-Cnt +, $n = 15$; and *Nanog*-Cnt +, $n = 15$). All error bars represent the standard error of measurements.

one stack every 10 s for 50 total time points (Figure 3B–D and Supplementary Movie S3). Because the number of theoretical recognition sites for MS2 and XA1.1 is 36 and >300, respectively, we observed relatively small and large dCas9-GFP spots that facilitated discrimination between the two loci (Figure 3B–E and Supplementary Movie S3). To explore the relationship between transcriptional activity and nuclear dynamics of pluripotency-related genes, we classified the cells into two groups, according to whether or not transcriptional MCP spots were observed during the imaging period. The mobility of *Oct4* did not show considerable differences with or without transcription during the imaging period, but that of *Nanog* showed obvious differences (Figure 3F). Although we quantified the mean dCas9-GFP fluorescent intensity in the nucleus of NMP-R cells with and without transcription during the imaging period, the intensity values of cells with transcription were comparable to those without transcription (Supplementary Figure S7), suggesting that changes in *Nanog* mobility is not caused by differences in dCas9-GFP expression levels.

In general, the free movement of an object can be confined in a nuclear or cellular compartment (25). This implies that the distance of any two points of the trajectory cannot exceed the maximal extension of the confining volume. Therefore, the MSD curves must reach a plateau at large time windows. Previously, Masui *et al.* analyzed the mobility of several loci, including the X-chromosome inactivation center, in mESCs over longer time periods (more than 2 h) and reported the diffusion coefficient of ∼0.007 μm^2/min and constrained radius of ∼1.7 μm, which is in the range of chromosome territories and well below the overall size of nucleus (32). In our analysis, we could not conclude with certainty whether the mobility of analyzed loci was also constrained, because apparent MSD plateaus were not observed until at least 400 s (Figure 3F). Diffusion coefficient in NMP-R cells (10 – 250 s) without *Nanog* transcription is 0.055 μm^2/min and, therefore, significantly higher ($P = 0.042$) than the value of the diffusion coefficient in cells with *Nanog* transcription ($D = 0.019$ μm^2/min).

To determine whether only the *Nanog-MS2* locus, only the XA1.1 locus, or both affected the mobility change in a transcription-dependent manner, the MSD was determined by measuring the mean squared change in the distance between dCas9-GFP spots and the nuclear center of mass on MCP-tdiRFP images (Figure 3E). The *Nanog* and XA1.1 loci in NMP-R cells showed a significantly higher mobility in the absence of *Nanog-MS2* transcription spots during the imaging period ($D = 0.062$ μm^2/min and $D = 0.039$ μm^2/min, respectively) than the loci in which transcription spots were present (*Nanog*, $D = 0.013$ μm^2/min, $P = 0.033$; XA1.1, $D = 0.0086$ μm^2/min, $P = 0.0053$) (Figure 3G and H). To compare these mobility changes to alterations of other genomic loci, we introduced telomere sgRNA expression vectors into NMP-R cells and determined MSD by measuring the mean squared change in distance between telomere dCas9-GFP spots and the nuclear center of mass on MCP-tdiRFP images (Figure 3E). No considerable difference in the mobility of telomeres was observed in cells with and without *Nanog* transcription during the imaging period (Figure 3G and H). Furthermore, in cells showing no *Nanog-MS2* transcription, the *Nanog* loci ($D = 0.062$ μm^2/min) showed nominally higher mobility than XA1.1 loci ($D = 0.039$ μm^2/min), although this effect did not reach statistical significance ($P = 0.20$). On the other hand, in OM-R cells, there was no such change in MSD according to the state of *Oct4-MS2* transactivation (Supplementary Figure S8).

mESCs can be brought to a ground state of pluripotency in which Nanog is more highly expressed (33). To induce this ground state, cells were treated with two inhibitors (2i) of MEK and GSK3β (27), and then motions of *Nanog-MS2* and XA1.1 loci were measured. Regardless of the absence of transcription during the imaging period, the mobility of *Nanog-MS2* and XA1.1 in NMP-R cells cultured in the 2i medium was lower than that of cells with transcriptional MCP spots cultured in the standard medium (Figure 3G and H). mESC populations cultured in the standard medium are comprised of metastable and multiple cellular states, including a ground state and a state in which mESCs are primed for differentiation (30). The former state is reported to have a significantly stiffer nucleus that is coupled to a globally more condensed chromatin state (34,35). Furthermore, it has been reported that genome mobility tends to increase during early mESC differentiation (32). Collectively, these results suggest that in the nuclei of mESCs in a non-ground state with lower *Nanog* transcriptional activity, a portion of the genomic region might have higher mobility compared to that in cells in the ground state.

DISCUSSION

Here, we described the ROLEX system, a live-imaging method for simultaneous measurements of the transcriptional activity and nuclear position of an endogenous gene. To analyze the relationship between genomic organization and transcription, RNA- and DNA-FISH are usually the techniques of choice (36,37). However, although RNA- and DNA-FISH enable simultaneous identification of the transcriptional state and specific gene loci in the nucleus, information on dynamic changes cannot be obtained because the sample needs to be fixated. In contrast, the use of fluorescent proteins fused to programmable DNA binding proteins, such as dCas9, transcription activator-like effector (TALE), and zinc finger (ZF), enables visualization of the nuclear organization in individual live cells (10,38–42). However, engineering ZF to bind to a specific sequence of interest is relatively difficult compared to TALE and sgRNA/dCas9 (43). Furthermore, the tendency of TALE to favor nucleolar localization hampers fluorescent labeling of genomic regions that are not highly repeated (39). Unlike TALE, the sgRNA/dCas9-GFP complex does not tend to localize to the nucleolus (Figure 1) and designing multiple sgRNAs for single-locus imaging is not laborious. One limitation of monitoring genomic organization using these live-imaging methods is that the relationship between the spatial organization of the genome and transcription of specific genes remains difficult to understand. Nevertheless, we believe that combining CRISPR imaging with the MS2 system (i.e. the ROLEX system) will allow quantification of both spatial and transcriptional dynamics of specific genes of interest.

In this study, only ∼6% of the NMP-R cells transduced with MS2 sgRNAs exhibited a dCas9-GFP spot corresponding to one of the *Nanog* DNA-FISH signals (Supplementary Figure S6). There could be two explanations for this low efficiency. Firstly, NMP-R cells showed cell-to-cell variability in levels of dCas9-GFP expression (Supplementary Figure S2). To control dCas9-GFP expression, we used a Tet system containing the rtTA2sM2 transactivator and the tTS(Kid) repressor (44). In this system, in the absence of the Dox treatment, tTS(Kid) represses the expression of the Tet responsive element (TRE)-regulated dCas9-GFP. In the presence of the Dox, tTS(Kid) unbinds from TRE, then rtTA2sM2 binds to TRE and activates dCas9-GFP expression. The use of this system is associated with irreversible inactivation of TRE-regulated genes and their heterogeneous expression in cells (45,46). However, it enables exploring the relationship between dCas9-GFP expression levels in individual cells and visualization of dCas9-GFP spots. To establish cell lines expressing dCas9-GFP at an optimum levels, weak promoters, such as TRE3G (Tet-On 3G system without Dox induction), can be used (10). Secondly, the maximum fluorescence intensity of dCas9-GFP obtained at the MS2 locus is relatively weak compared to other loci (XA1.1, telomere and MiSat). In CRISPR imaging, the accumulation of dCas9-GFP at a genomic locus of interest causes spot signal intensity to rise above the background (10). Therefore, too little or too much dCas9-GFP expression hampers the detection of target spot signals (Supplementary Figure S6). Furthermore, we found that dCas9-GFP signal intensity dynamically changed (Supplementary Figure S5). At the same time, dynamic signal changes were not clearly observed in cells transfected with telomere, MiSat, and XA1.1 sgRNA expression vectors (data not shown). Theoretical numbers of sgRNA/dCas9-GFP binding sites in these highly repeated regions is variable. Telomere length is 60 kb and it comprises about 2500 binding sites on average (47); MiSat length is 0.5–1.2 Mb, which is compatible with several thousand binding sites (48); XA1.1 sgRNAs theoretically bind to more than 300 sites within the XA1.1 locus. All these loci contain many more binding sites than the total of 36 sgRNA/dCas9-GFP binding sites within an MS2 repeat, which suggests that the presence of a larger number of binding sites increases signal-to-noise ratio and results in a robust spot signal. Conversely, dCas9-GFP spot signals in cells expressing sgRNAs with smaller target sites (e.g. MS2 sgRNAs) can be affected by stochastic binding and unbinding, binding competition between dCas9-GFP and other DNA binding proteins and fluorescent bleaching. It might be also possible that the movement of spots with a lower signal-to-noise ratio in and out of focus could affect signal fluctuations. Increase in the signal-to-noise ratio at an MS2 repeat can be achieved by the increase in the number of MS2 sites in the repeat, the use of multiple fluorescent proteins fused in tandem (42), or SunTag, which can recruit multiple copies of the fluorescent protein (49).

Our results suggest that the MS2 sgRNA/dCas9-GFP complex dissociates from its target site by transcription mediated by RNA Pol II. This conclusion is based on the observation that MS2 sgRNA/dCas9-GFP spot signals tended to decrease or disappear when a strong MCP-tdiRFP spot signal was detected (Supplementary Movies S2). Therefore, if the ROLEX system is applied to genes with much higher expression levels than *Nanog*, it is possible that MS2 sgRNA/dCas9-GFP spots may become difficult to detect. As mentioned before, this fact requires further clarification. Nevertheless, with the current system, nuclear localization of the target gene can still be determined with high confidence through the MCP-tdiRFP spot signal. Hence, we believe that there is room for improving the dynamic range of the transcript-detection component of the ROLEX system, towards a more robust application for the simultaneous quantification of transcriptional activity and nuclear localization of genes in living cells.

ROLEX enabled the detection of sub-genome-wide mobility changes depending on the state of *Nanog* transactivation in mESCs. The fact that mobility changes were observed only in a part of the nucleus might be explained by the differences in long-range genomic interactions. The *Nanog* promoter region has been shown to be physically associated with multiple and distal intrachromosomal regions (3). Furthermore, we recently found that *Nanog* promoter states stochastically switch ON and OFF, and that the transcription rate during the ON state is almost constant (17). Therefore, if *Nanog* interacts with multiple distal regions, it would show a lower mobility and be stably transcribed for 2–3 min (on average) in mESCs with higher *Nanog* transcriptional activity (17). On the other hand, if the *Nanog* gene does not interact with multiple distal regions, it would show a higher mobility in mESCs with lower *Nanog* transcriptional activity. It is possible that such a change in the number of interactions stochastically occurs in a genomic region-specific manner, leading to a sub-genome-wide mobility change, monoallelic expression on *Nanog* (29), and cell-to-cell heterogeneity in gene expression (6) in mESCs. Single-cell analysis of transcription and nuclear dynamics using the ROLEX system could be instrumental for gaining a valuable insignt into the mechanisms underlying the maintenance of pluripotency and cell-to-cell heterogeneity in gene expression.

Recent progress in 3C-related technologies (4C, 5C and Hi-C) revealed three-dimensional genomic organization of several cell types from diverse organisms, including mESCs, with many long-range genomic interactions being implicated into the regulation of gene expression (1–4). To understand such complexity of gene regulation, multicolor imaging with more than two colors, such as dCas9-GFP and MCP-tdiRFP, might be required. For RNA imaging, the λN22 system (50) could be used as well as MS2 system. Furthermore, multicolor versions of CRISPR using dCas9 of different origins has been recently reported (42). We expect that a combined use of these tools might enable us to explore the complex gene regulation via dynamic long-range interactions.

In summary, we have described the ROLEX system, which can be applied for simultaneous imaging of the transcription and nuclear position of an endogenous gene. We believe that, among other uses, this system could be employed to investigate whether variability in the genomic organization of cells causes cell-to-cell heterogeneity in gene expression, and to study the dynamics of gene regulation via long-range genomic interactions. Although integration of the MS2 repeat into a specific genomic site is required

for the utilization of the ROLEX system, this is no longer a laborious task owing to recent advances in genome editing using programmable endonucleases (43). It is expected that by enabling exploration of the relationship between transcription and nuclear dynamics in living cells, the ROLEX system will become a powerful tool not only in cell biology but also in other fields including biomedical research and clinical therapy.

SUPPLEMENTARY DATA

Supplementary Data are available at NAR Online.

ACKNOWLEDGEMENTS

We would like to thank Dr Connie Cepko for supplying the pCAG-Cre vector (Addgene plasmid 13775); Dr Allan Bradley for supplying the pPB-LR5 vector, Dr Nancy L. Craig for supplying the pCMV-hyPBase vector, Dr Kosuke Yusa for supplying the pKLV-U6gRNA(BbsI)-PGKpuro2ABFP vector (Addgene plasmid 50946), Dr Feng Zhang for supplying the pX335-U6-Chimeric_BB-CBh-hSpCas9n(D10A) vector (Addgene plasmid 42335) and Ms.Noriko Sumiyoshi for technical assistance.

FUNDING

Platform for Dynamic Approaches to Living System from the Ministry of Education, Culture, Sports, Science and Technology of Japan [to H.O., T.S. and T.Y.]; Grants-in-Aid for Scientific Research from the Ministry of Education, Culture, Sports, Science and Technology [25830138 and 15K18467 to H.O.]. Funding for open access charge: Platform for Dynamic Approaches to Living System from the Ministry of Education, Culture, Sports, Science and Technology of Japan.
Conflict of interest statement. None declared.

REFERENCES

1. Dekker,J., Marti-Renom,M.A. and Mirny,L.A. (2013) Exploring the three-dimensional organization of genomes: interpreting chromatin interaction data. *Nat. Rev. Genet.*, **14**, 390–403.
2. Dixon,J.R., Selvaraj,S., Yue,F., Kim,A., Li,Y., Shen,Y., Hu,M., Liu,J.S. and Ren,B. (2012) Topological domains in mammalian genomes identified by analysis of chromatin interactions. *Nature*, **485**, 376–380.
3. de Wit,E., Bouwman,B.A.M., Zhu,Y., Klous,P., Splinter,E., Verstegen,M.J.A.M., Krijger,P.H.L., Festuccia,N., Nora,E.P., Welling,M. *et al.* (2013) The pluripotent genome in three dimensions is shaped around pluripotency factors. *Nature*, **501**, 227–231.
4. Phillips-Cremins,J.E., Sauria,M.E.G., Sanyal,A., Gerasimova,T.I., Lajoie,B.R., Bell,J.S.K., Ong,C.-T., Hookway,T.A., Guo,C., Sun,Y. *et al.* (2013) Architectural protein subclasses shape 3D organization of genomes during lineage commitment. *Cell*, **153**, 1281–1295.
5. Schoenfelder,S., Sexton,T., Chakalova,L., Cope,N.F., Horton,A., Andrews,S., Kurukuti,S., Mitchell,J.A., Umlauf,D., Dimitrova,D.S. *et al.* (2010) Preferential associations between co-regulated genes reveal a transcriptional interactome in erythroid cells. *Nat. Genet.*, **42**, 53–61.
6. Noordermeer,D., de Wit,E., Klous,P., van de Werken,H., Simonis,M., Lopez-Jones,M., Eussen,B., de Klein,A., Singer,R.H. and de Laat,W. (2011) Variegated gene expression caused by cell-specific long-range DNA interactions. *Nat. Cell Biol.*, **13**, 944–951.
7. Nagano,T., Lubling,Y., Stevens,T.J., Schoenfelder,S., Yaffe,E., Dean,W., Laue,E.D., Tanay,A. and Fraser,P. (2014) Single-cell Hi-C reveals cell-to-cell variability in chromosome structure. *Nature*, **502**, 59–64.
8. Giorgetti,L., Galupa,R., Nora,E.P., Piolot,T., Lam,F., Dekker,J., Tiana,G. and Heard,E. (2014) Predictive Polymer Modeling Reveals Coupled Fluctuations in Chromosome Conformation and Transcription. *Cell*, **157**, 950–963.
9. Hocine,S., Raymond,P., Zenklusen,D., Chao,J.A. and Singer,R.H. (2012) Single-molecule analysis of gene expression using two-color RNA labeling in live yeast. *Nat. Methods*, **10**, 119–121.
10. Chen,B., Gilbert,L.A., Cimini,B.A., Schnitzbauer,J., Zhang,W., Li,G.-W., Park,J., Blackburn,E.H., Weissman,J.S., Qi,L.S. *et al.* (2013) Dynamic imaging of genomic locin living human cells by an optimized CRISPR/Cas system. *Cell*, **155**, 1479–1491.
11. Yusa,K., Rad,R., Takeda,J. and Bradley,A. (2009) Generation of transgene-free induced pluripotent mouse stem cells by the piggyBac transposon. *Nat. Methods*, **6**, 363–369.
12. Shaner,N.C., Lambert,G.G., Chammas,A., Ni,Y., Cranfill,P.J., Baird,M.A., Sell,B.R., Allen,J.R., Day,R.N., Israelsson,M. *et al.* (2013) A bright monomeric green fluorescent protein derived from Branchiostoma lanceolatum. *Nat. Methods*, **10**, 407–409.
13. Yusa,K., Zhou,L., Li,M.A., Bradley,A. and Craig,N.L. (2011) A hyperactive piggyBac transposase for mammalian applications. *Proc. Natl. Acad. Sci. U.S.A.*, **108**, 1531–1536.
14. Koike-Yusa,H., Li,Y., Tan,E.-P., Velasco-Herrera,M.D.C. and Yusa,K. (2014) Genome-wide recessive genetic screening in mammalian cells with a lentiviral CRISPR-guide RNA library. *Nat. Biotechnol.*, **32**, 267–273.
15. Ran,F.A., Hsu,P.D., Wright,J., Agarwala,V., Scott,D.A. and Zhang,F. (2013) Genome engineering using the CRISPR-Cas9 system. *Nat. Protoc.*, **8**, 2281–2308.
16. Cong,L., Ran,F.A., Cox,D., Lin,S., Barretto,R., Habib,N., Hsu,P.D., Wu,X., Jiang,W., Marraffini,L.A. *et al.* (2013) Multiplex genome engineering using CRISPR/Cas systems. *Science*, **339**, 819–823.
17. Ochiai,H., Sugawara,T., Sakuma,T. and Yamamoto,T. (2014) Stochastic promoter activation affects Nanog expression variability in mouse embryonic stem cells. *Sci. Rep.*, **4**, 7125.
18. Matsuda,T. and Cepko,C.L. (2007) Controlled expression of transgenes introduced by in vivo electroporation. *Proc. Natl. Acad. Sci. U.S.A.*, **104**, 1027–1032.
19. Ochiai,H., Miyamoto,T., Kanai,A., Hosoba,K., Sakuma,T., Kudo,Y., Asami,K., Ogawa,A., Watanabe,A., Kajii,T. *et al.* (2014) TALEN-mediated single-base-pair editing identification of an intergenic mutation upstream of BUB1B as causative of PCS (MVA) syndrome. *Proc. Natl. Acad. Sci. U.S.A.*, **111**, 1461–1466.
20. Bolland,D.J., King,M.R., Reik,W., Corcoran,A.E. and Krueger,C. (2013) Robust 3D DNA FISH using directly labeled probes. *J. Vis. Exp.*, doi:10.3791/50587.
21. Carpenter,A.E., Jones,T.R., Lamprecht,M.R., Clarke,C., Kang,I.H., Friman,O., Guertin,D.A., Chang,J.H., Lindquist,R.A., Moffat,J. *et al.* (2006) CellProfiler: image analysis software for identifying and quantifying cell phenotypes. *Genome Biol.*, **7**, R100.
22. Livak,K.J. and Schmittgen,T.D. (2001) Analysis of relative gene expression data using real-time quantitative PCR and the 2(-Delta Delta C(T)) Method. *Methods*, **25**, 402–408.
23. Vazquez,J., Belmont,A.S. and Sedat,J.W. (2001) Multiple regimes of constrained chromosome motion are regulated in the interphase Drosophila nucleus. *Curr. Biol.*, **11**, 1227–1239.
24. Berg,H.C. (1993) *Random Walks in Biology*, Princeton University Press. Princeton, NJ.
25. Carmo-Fonseca,M., Platani,M. and Swedlow,J.R. (2002) Macromolecular mobility inside the cell nucleus. *Trends Cell Biol.*, **12**, 491–495.
26. Guenatri,M., Bailly,D., Maison,C. and Almouzni,G. (2004) Mouse centric and pericentric satellite repeats form distinct functional heterochromatin. *J. Cell Biol.*, **166**, 493–505.
27. Ying,Q.-L., Wray,J., Nichols,J., Batlle-Morera,L., Doble,B., Woodgett,J., Cohen,P. and Smith,A. (2008) The ground state of embryonic stem cell self-renewal. *Nature*, **453**, 519–523.
28. Qi,L.S., Larson,M.H., Gilbert,L.A., Doudna,J.A., Weissman,J.S., Arkin,A.P. and Lim,W.A. (2013) Repurposing CRISPR as an RNA-guided platform for sequence-specific control of gene expression. *Cell*, **152**, 1173–1183.

29. Miyanari,Y. and Torres-Padilla,M.-E. (2012) Control of ground-state pluripotency by allelic regulation of Nanog. *Nature*, **483**, 470–473.
30. Singer,Z.S., Yong,J., Tischler,J., Hackett,J.A., Altinok,A., Surani,M.A., Cai,L. and Elowitz,M.B. (2014) Dynamic heterogeneity and DNA methylation in embryonic stem cells. *Mol. Cell*, **55**, 319–331.
31. Cabal,G.G., Genovesio,A., Rodriguez-Navarro,S., Zimmer,C., Gadal,O., Lesne,A., Buc,H., Feuerbach-Fournier,F., Olivo-Marin,J.-C., Hurt,E.C. *et al.* (2006) SAGA interacting factors confine sub-diffusion of transcribed genes to the nuclear envelope. *Nature*, **441**, 770–773.
32. Masui,O., Bonnet,I., Le Baccon,P., Brito,I., Pollex,T., Murphy,N., Hupé,P., Barillot,E., Belmont,A.S. and Heard,E. (2011) Live-cell chromosome dynamics and outcome of X chromosome pairing events during ES cell differentiation. *Cell*, **145**, 447–458.
33. Kalmar,T., Lim,C., Hayward,P., Muñoz-Descalzo,S., Nichols,J., Garcia-Ojalvo,J. and Martinez-Arias,A. (2009) Regulated fluctuations in nanog expression mediate cell fate decisions in embryonic stem cells. *PLoS Biol.*, **7**, e1000149.
34. Chalut,K.J., Höpfler,M., Lautenschläger,F., Boyde,L., Chan,C.J., Ekpenyong,A., Martinez-Arias,A. and Guck,J. (2012) Chromatin decondensation and nuclear softening accompany nanog downregulation in embryonic stem cells. *Biophys. J.*, **103**, 2060–2070.
35. Pagliara,S., Franze,K., McClain,C.R., Wylde,G.W., Fisher,C.L., Franklin,R.J.M., Kabla,A.J., Keyser,U.F. and Chalut,K.J. (2014) Auxetic nuclei in embryonic stem cells exiting pluripotency. *Nat. Mater.*, **13**, 638–644.
36. Lawrence,J.B. and Singer,R.H. (1991) Spatial organization of nucleic acid sequences within cells. *Semin. Cell Biol.*, **2**, 83–101.
37. Clemson,C.M. and Lawrence,J.B. (1996) Multifunctional compartments in the nucleus: insights from DNA and RNA localization. *J. Cell. Biochem.*, **62**, 181–190.
38. Lindhout,B.I., Fransz,P., Tessadori,F., Meckel,T., Hooykaas,P.J.J. and van der Zaal,B.J. (2007) Live cell imaging of repetitive DNA sequences via GFP-tagged polydactyl zinc finger proteins. *Nucleic Acids Res.*, **35**, e107.
39. Miyanari,Y., Ziegler-Birling,C. and Torres-Padilla,M.-E. (2013) Live visualization of chromatin dynamics with fluorescent TALEs. *Nat. Struct. Biol.*, **20**, 1321–1324.
40. Thanisch,K., Schneider,K., Morbitzer,R., Solovei,I., Lahaye,T., Bultmann,S. and Leonhardt,H. (2014) Targeting and tracing of specific DNA sequences with dTALEs in living cells. *Nucleic Acids Res.*, **42**, e38.
41. Ma,H., Reyes-Gutierrez,P. and Pederson,T. (2013) Visualization of repetitive DNA sequences in human chromosomes with transcription activator-like effectors. *Proc. Natl. Acad. Sci. U.S.A.*, **110**, 21048–21053.
42. Ma,H., Naseri,A., Reyes-Gutierrez,P., Wolfe,S.A., Zhang,S. and Pederson,T. (2015) Multicolor CRISPR labeling of chromosomal loci in human cells. *Proc. Natl. Acad. Sci. U.S.A.*, **112**, 3002–3007.
43. Carroll,D. (2014) Genome engineering with targetable nucleases. *Annu. Rev. Biochem.*, **83**, 409–439.
44. Xiong,W., Goverdhana,S., Sciascia,S.A., Candolfi,M., Zirger,J.M., Barcia,C., Curtin,J.F., King,G.D., Jaita,G., Liu,C. *et al.* (2006) Regulatable gutless adenovirus vectors sustain inducible transgene expression in the brain in the presence of an immune response against adenoviruses. *J. Virol.*, **80**, 27–37.
45. Barde,I., Zanta-Boussif,M.A., Paisant,S., Leboeuf,M., Rameau,P., Delenda,C. and Danos,O. (2006) Efficient control of gene expression in the hematopoietic system using a single Tet-on inducible lentiviral vector. *Mol. Ther.*, **13**, 382–390.
46. Ying,Y., Yang,X., Zhao,K., Mao,J., Kuang,Y., Wang,Z., Sun,R. and Fei,J. (2015) The Krüppel-associated box repressor domain induces reversible and irreversible regulation of endogenous mouse genes by mediating different chromatin states. *Nucleic Acids Res.*, **43**, 1549–1561.
47. García-Cao,M., O'Sullivan,R., Peters,A.H.F.M., Jenuwein,T. and Blasco,M.A. (2004) Epigenetic regulation of telomere length in mammalian cells by the Suv39h1 and Suv39h2 histone methyltransferases. *Nat. Genet.*, **36**, 94–99.
48. Kuznetsova,I.S., Prusov,A.N., Enukashvily,N.I. and Podgornaya,O.I. (2005) New types of mouse centromeric satellite DNAs. *Chromosome Res.*, **13**, 9–25.
49. Tanenbaum,M.E., Gilbert,L.A., Qi,L.S., Weissman,J.S. and Vale,R.D. (2014) A protein-tagging system for signal amplification in gene expression and fluorescence imaging. *Cell*, **159**, 635–646.
50. Urbanek,M.O., Galka-Marciniak,P., Olejniczak,M. and Krzyzosiak,W.J. (2014) RNA imaging in living cells – methods and applications. *RNA Biol.*, **11**, 1083–1095.
51. Das,S., Jena,S. and Levasseur,D.N. (2011) Alternative splicing produces Nanog protein variants with different capacities for self-renewal and pluripotency in embryonic stem cells. *J. Biol. Chem.*, **286**, 42690–42703.